Supporting information

Improved Charge Delivery within Covalently Ligated Cobalt Phthalocyanine Electrocatalyst for CO_2 Reduction

Alena S. Kochubei[a], Aleksei N. Marianov[a], Yuming Wu[a], Mengxin Liu[a], Haoyue Sun[b], Jun Huang [b], Oliver J. Conquest[c], Teng Lu,[d] Yun Liu,[d] Catherine Stampfl[c] and Yijiao Jiang[a, *]

[a] School of Engineering, Macquarie University, Sydney, NSW 2109, Australia

[b] School of Chemical and Biomolecular Engineering, The University of Sydney, NSW 2006, Australia

[c] School of Physics, The University of Sydney, NSW 2006, Australia

[d] Research School of Chemistry, The Australian National University, Canberra, ACT 0200, Australia

* To whom correspondence should be addressed:
Tel: +612-9850-9535
Fax: +612-9850-9128
E-mail: yijiao.jiang@mq.edu.au

Contents

1. Additional methods of characterization

^{1}H NMR spectra were collected on a Bruker Avance III 600 MHz spectrometer. The chemical shifts were referenced against residual DMSO-d_6 signals (δ = 2.50 ppm). High resolution mass spectra (HRMS) were recorded on an ESI MS Q Exactive™ Plus hybrid quadrupole-Orbitrap mass spectrometer (Thermo Fisher Scientific). ICP-MS analysis of the Co content was conducted on Agilent 7500 ICPMS spectrometer.

2. Calculations

The amount of electrochemically active complex was calculated by the integration of the first oxidation wave (Equation S1): [1]

$$\Gamma_{EA} = \frac{Q_{CV}}{nFA} \quad \text{(S1)}$$

where Q_{CV} – charge found from the integration of Co^{II}/Co^{I} reduction peak (C), n – number of electrons transferred in the reaction (1 in this case), F – Faraday's constant (96485 C/mol), A – electrode area (cm^2).

Turnover frequencies (TOFs) for CO were determined using Equation S2:

$$TOF = \frac{n_i}{\Gamma_{EA} A \tau} \quad \text{(S2)}$$

where n_i – the amount of CO or H_2 measured with gas chromatography (GC) at a given time (mol), τ – reaction time (s).

Selectivity to CO was calculated from Equation S3:

$$FE_{CO} = 100\frac{n_{co}}{n_{CO} + n_{H_2}} \quad \text{(S3)}$$

3. Synthesis of phthalocyanines

***5-nitro-1,3-diiminoisoindoline* (2)**

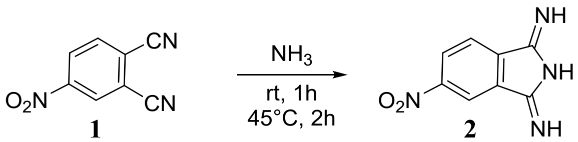

Figure S1. Synthesis of 5-nitro-1,3-diiminoisoindoline.

4-nitro-1,2-dicyanobenzene **1** (692.5 mg, 4.000 mmol) and potassium tert-butoxide (44.9 mg, 0.400 mmol) were dissolved in 40 mL of methanol under stirring at room temperature. The solution was saturated with ammonia using a gentle stream of dry NH_3 (the stream was dried with pellets of KOH) at room temperature and 30 min later the temperature was increased to 45°C. After 30 min of stirring under the flow of NH_3, the product started to precipitate from the solution. The reaction was monitored by thin-layer chromatography (TLC) using ethyl acetate as a mobile phase. After 1.5 h the gas flow was stopped and the greenish-yellow crystalline solid was filtered off giving 586.8 mg of product - diiminoisoindoline **2** (77%). After the evaporation of methanol to 10 mL, an additional 84.0 mg of solid was collected bringing the final yield to 670.8 mg (88.0 %). IR signals are in agreement with the previously reported data.[2] **Notes:** The **1** should be dissolved completely before the potassium tert-butoxide is added to the solution under vigorous stirring. The mixture becomes greenish at the beginning and must be purged with NH_3 at room temperature until it turns yellow again. The ^{1}H NMR spectrum of 5-nitro-1,3-diiminoisoindoline is shown in Figure S2.

IR(neat, cm^{-1}): 3363(-NH), 3253(-NH), 3096(C-H), 1686, 1642, 1546, 1513(-NO_2), 1343(-NO_2), 1297, 1130, 891(benzene ring), 802(meta-substitution), 752(meta-substitution), 701(meta-substitution)

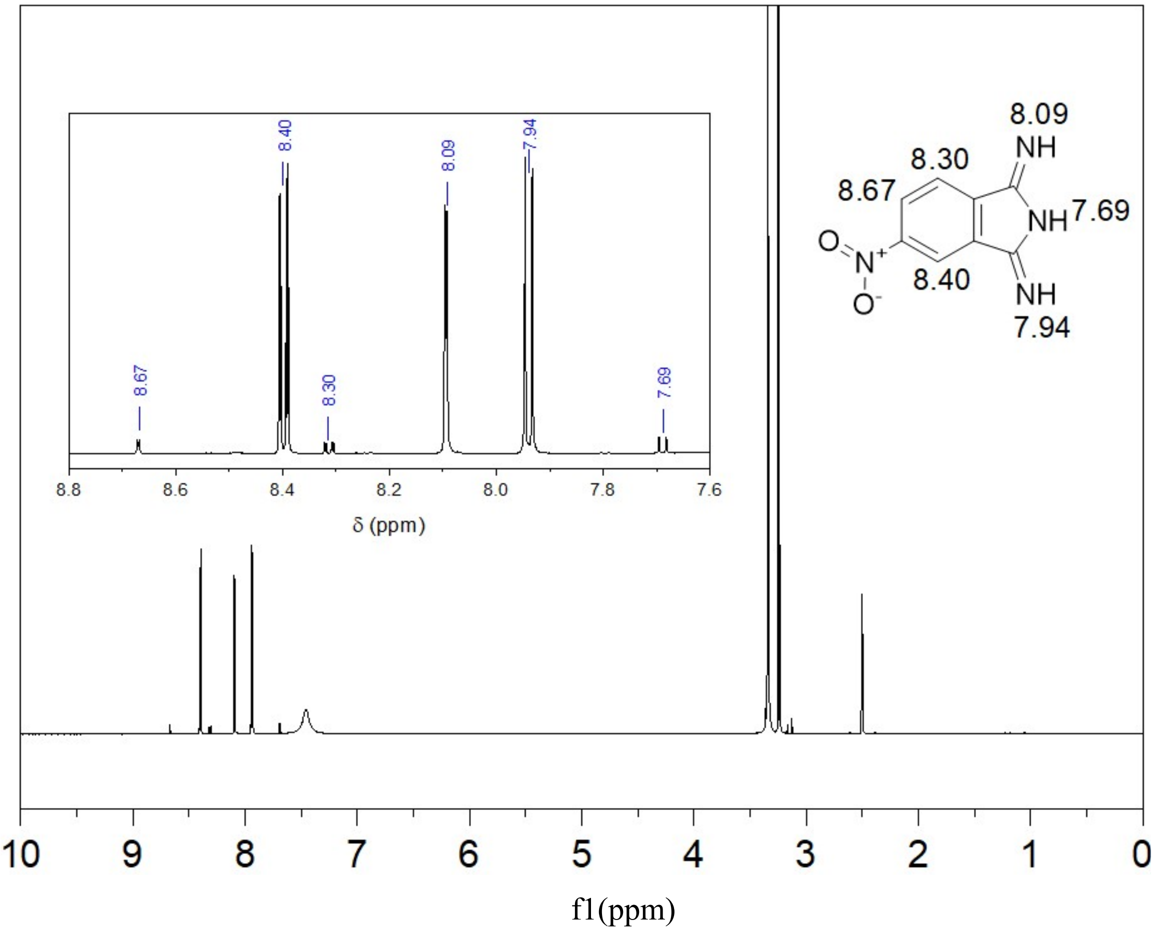

Figure S2. ¹H NMR spectrum of 5-nitro-1,3-diiminoisoindoline (DMSO-d6, 600 MHz).

Tetrakis nitrophthalocyanine (**t-NO_2Pc**)

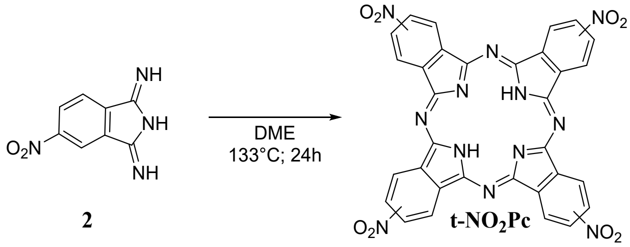

Figure S3. Synthesis of tetra-nitrophthalocyanine (**t-NO_2Pc**).

The method used is based on the patented procedure.[3] Crude product of 5-nitro-1,3-diiminoisoindoline **2** synthesis (0.600 g, 3.200 mmol) was mixed with 4 mL of *N,N*-dimethylaminoethanol in a 25 mL round-bottom flask. The vessel was topped up with a condenser and the contents were brought to a boil. The mixture was refluxed under constant stirring for 24 h and was cooled down. The precipitate was filtered off and washed with acetone (2 times) and ethanol (2 times). A dark green solid was dried under vacuum overnight. Yield - 0.5 g (91.2 %, 0.720 mmol). IR signals are in agreement with the previously reported data.[4]

IR(neat, cm^{-1}): 3364(-NH), 3253(-NH), 3093(C-H), 1513(-NO_2), 1338(-NO_2), 1298, 1131, 1125, 1070, 895(benzene ring), 843(meta substitution), 803(meta substitution),738(meta substitution), 702(meta substitution).

The ^{1}H NMR spectrum of **t-NO_2Pc** is shown in Figure S4. The S/N for the free-base phthalocyanines is very low due to extremely poor solubility of the products. The large signals at 3.32 and 2.50 ppm correspond to the water and residual DMSO-d_6, respectively. The minor peaks arise from the minor amounts of solvents stuck in the crystalline structure of the product as well as ^{13}C-^{1}H satellites. The aromatic signals of **t-NO_2Pc** do not resolve into the clear multiplets since the synthesised product is a mixture of regioisomers.

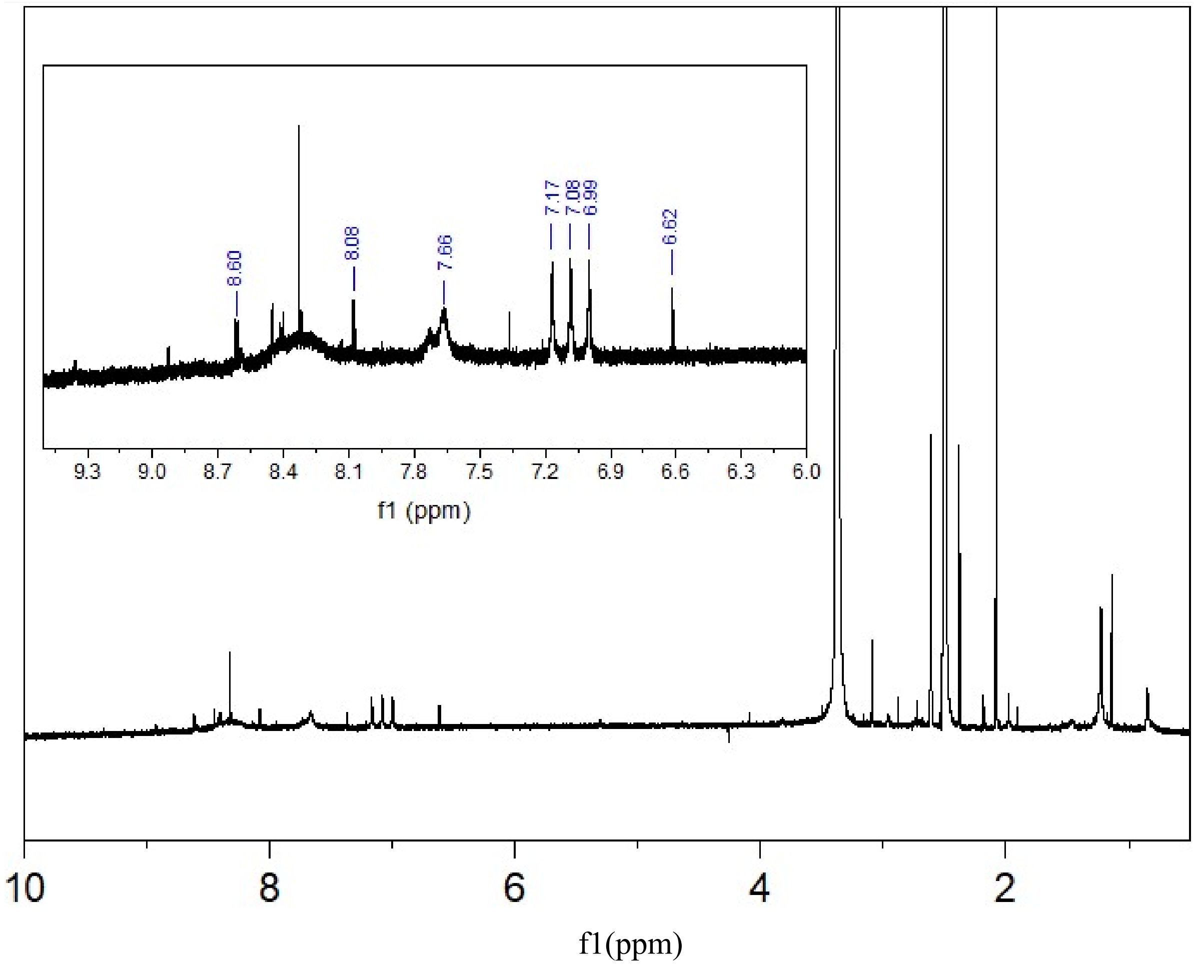

Figure S4. [1]H NMR spectrum of tetra-nitrophthalocyanine **t-NO_2Pc** (DMSO-d6, 600 MHz).

Tetra-aminophthalocyanine (t-NH_2Pc)

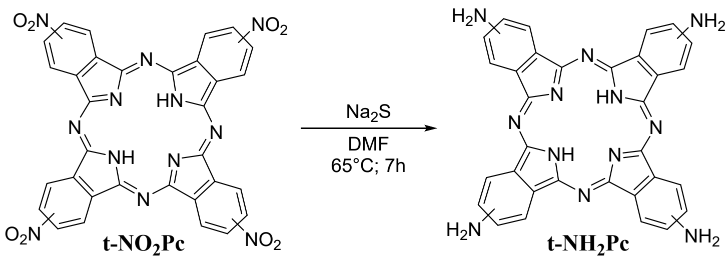

Figure S5. Synthesis of tetra-aminophthalocyanine (**t-NH_2Pc**).

The procedure used is based on the previously reported method.[4] Tetra-nitrophthalocyanine (428.5 mg, 0.616 mmol) and sodium sulphide nonahydrate (1.868 g, 7.626 mmol) were mixed with 12 mL of N,N-dimethylformamide (DMF). The mixture was kept at 65°C for 7 h under stirring. Then it was dispersed in 37 mL of ice-cold water and the solid was filtered off. A dark green product was washed with 10 mL of methanol 5 times and dried under reduced pressure overnight. The resulting phthalocyanine was then redispersed in methanol and boiled for 2 h. The precipitate was filtered off and dried in a vacuum overnight. Yield - 267.7 mg (75.4 %).

HRMS (ESI) $[M]^+$ calculated for $C_{32}H_{22}N_{12}$, 574.2085; found 574.2080.

^{1}H NMR spectrum of **t-NH_2Pc** is shown in Figure S6, in good agreement with the data reported previously.[4]. Similar to **t-NO_2Pc**, the S/N is low due to the poor solubility of **t-NH_2Pc**. Nevertheless, the success of the synthesis is evident from the strong upfield shift of the aromatic signals occurring after the treatment of the tetra-nitrophthalocyanine with the reductant.

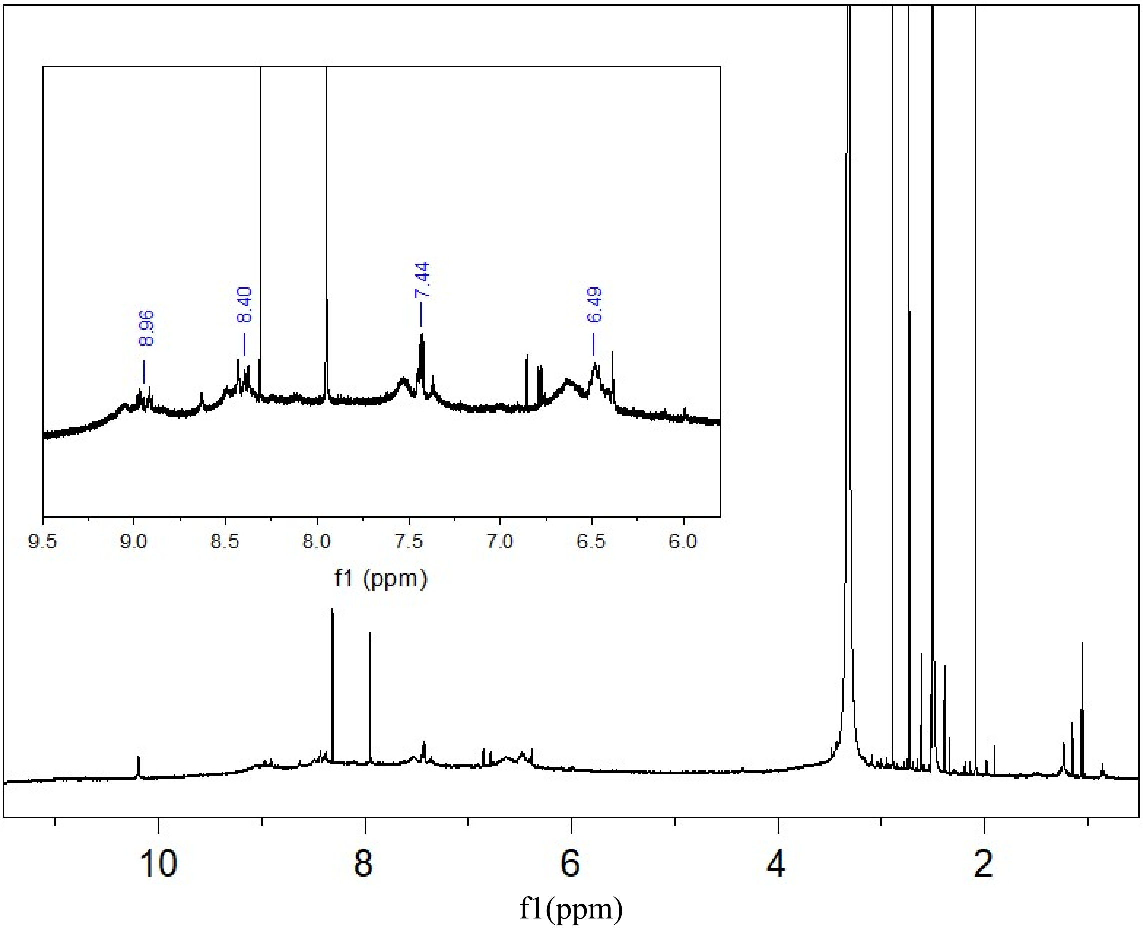

Figure S6. ^{1}H NMR spectrum of tetra-aminophthalocyanine **t-NH$_2$Pc** (DMSO-d6, 600 MHz).

4. Electrochemical grafting of the Pc ligand on CFP

Electrochemical covalent ligation of the Pc ligand was performed based on the procedure reported earlier.[5] It is schematically demonstrated in Figure S7:

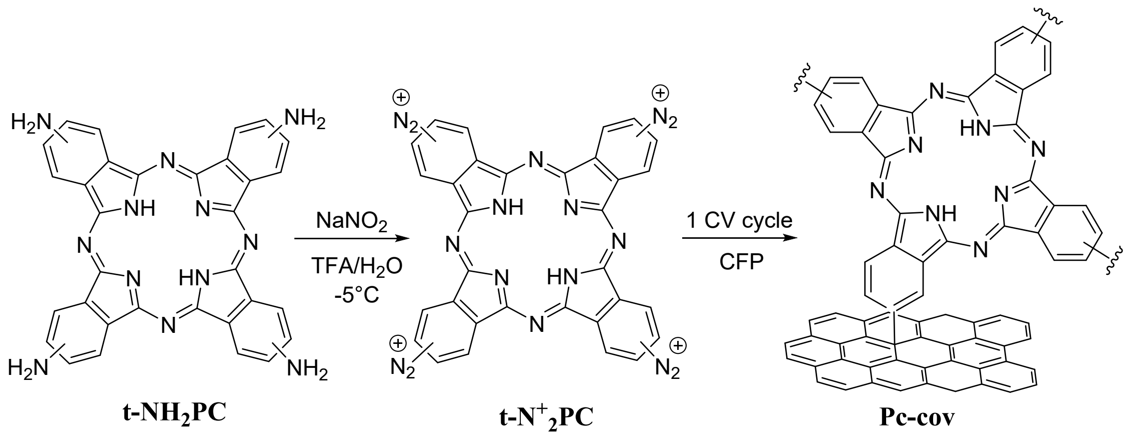

Figure S7. Covalent ligation of the Pc ligand on the surface of CFP.

The grafting of the Pc moieties is evident from the dramatic increase of the reductive current in the presence of **t-NH$_2$Pc** compared to a blank experiment containing only free-base phthalocyanine (Figure S8).[6]

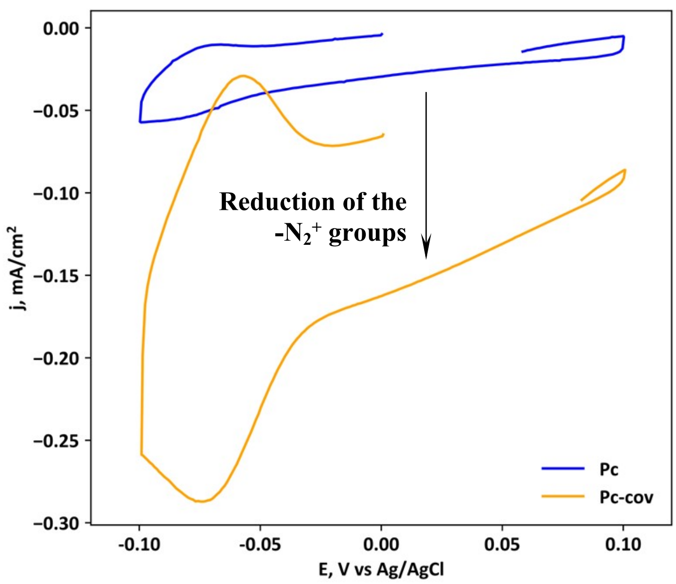

Figure S8. CV recorded during the electrochemical reduction of **t-N$_2^+$Pc** (orange) and a free-base Pc (blue). The increase of the current demonstrates the reductive decomposition of the -N$_2^+$ moieties.

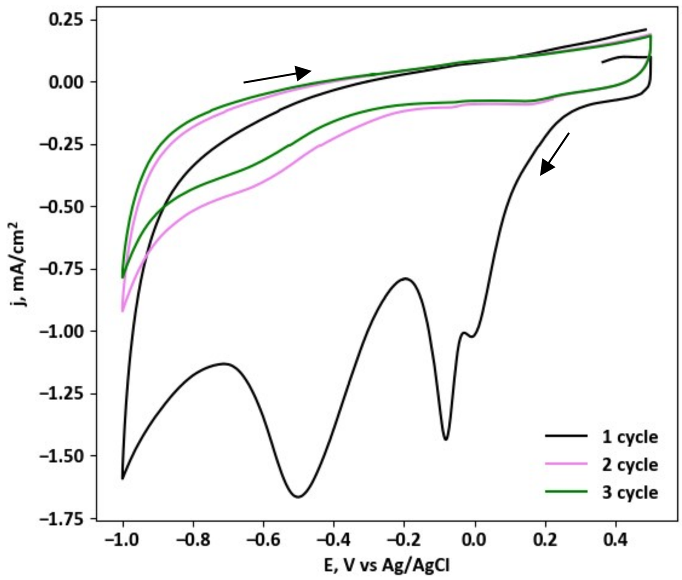

Figure S9. 3 CV cycles recorded during the electrochemical reduction of **t-N_2^+Pc** (orange). The absence of the peaks on the reoxidation wave demonstrates the irreversibility of the **t-N_2^+Pc** reduction.

5. AFM

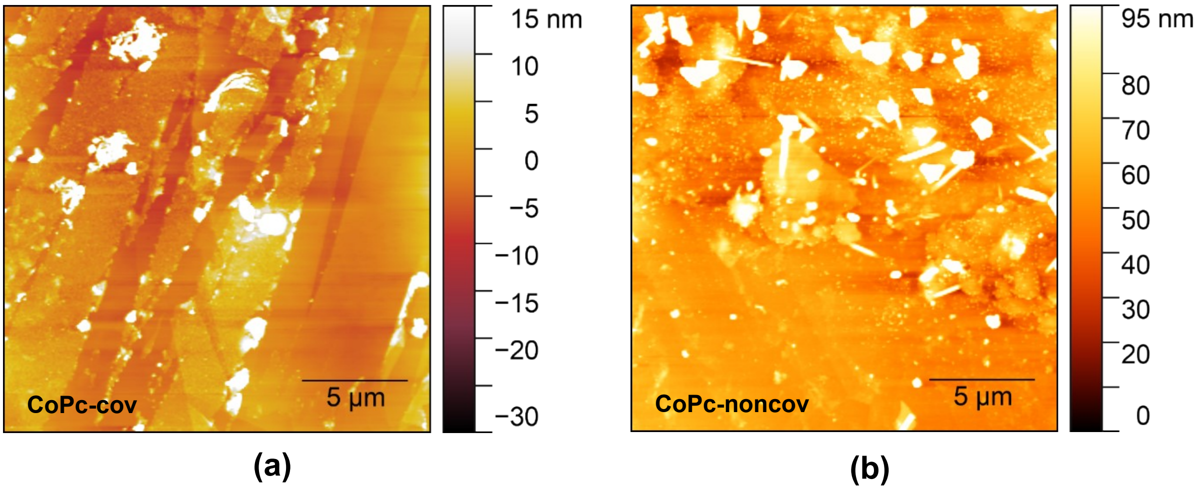

Figure S10. Topographic images of (**a**) **CoPc-cov** and (**b**) **CoPc-noncov** immobilized on HOPG.

6. Raman signals assignment

Table S1. Comparison of Raman spectra of CoPc purchased from Sigma Aldrich (CoPc, Sigma), **CoPc-noncov,** and **CoPc-cov** with the previously reported data (CoPc and CoPc-Py).

Assignment of the signals[7]	CoPc [7]	CoPc, Sigma	CoPc -Py[7]	CoPc-noncov	CoPc-cov
	591	593	591	591	
		632			
	680	681	680	681	
	720	720			
B1g; ν(Co57-Ni) + σ(Ca-Nb-Ca) + exp (pyrrole)	750	748	750	748	752
	793	779			
	834	830	832	833	
	889	low int			
B2g; ν(ring) + σ(Ni-Co57-Ni) + def (benzene)	958	957	957	958	
	1082	1007			
Eu; ν(Co57-Ni)+ ν(isoindole) +σ(C-H)	1106	1106	1105	1107	
	1139	1137	1137	1138	
	1161	low int	1161	1161	
B2g; ν(Ca-Ni) + σ(Cc-H) + σ(Ni-Co57-Ni)	1191	1187	1191	1191	
B1g; ν(Co57-Ni) + ν(isoindole) + σ(C-H)	1308	1305	1306	1306	
	1339	1336	1335	1345	
A1g; ν(Co57-Ni) + ν(Cd-Cd) + σ(Ca-Nb-Ca) + σ(Cc-H)	1425	1434			
	1450	1450		1450	
B2g; σ(C-H) + def (isoindole)	1465	1459	1460	1460	1460
		1491			
B1g; ν(Ca-Nb) + σ(C-H)+ exp (pyrrole)	1539	1531	1532	1535	1540

7. Raman signals of -OH groups

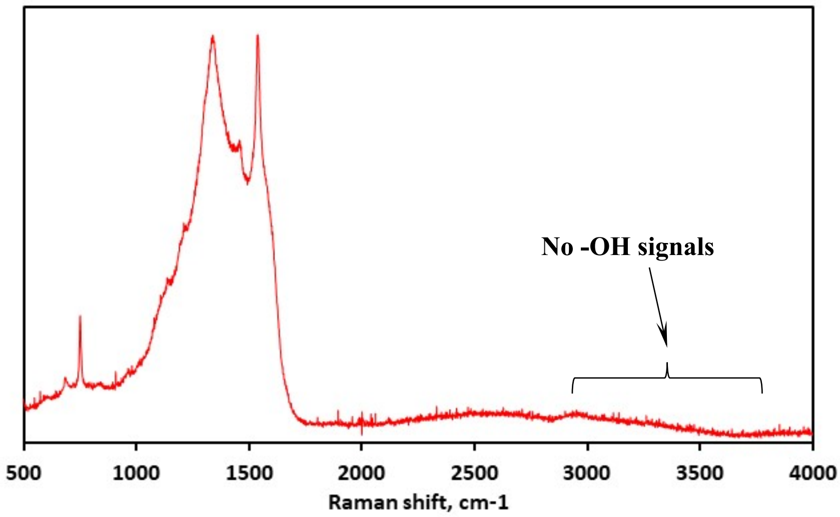

Figure S11. Raman spectrum of **CoPc-cov** in the range of 500-4000 nm.

8. XPS analysis of CoPc-cov

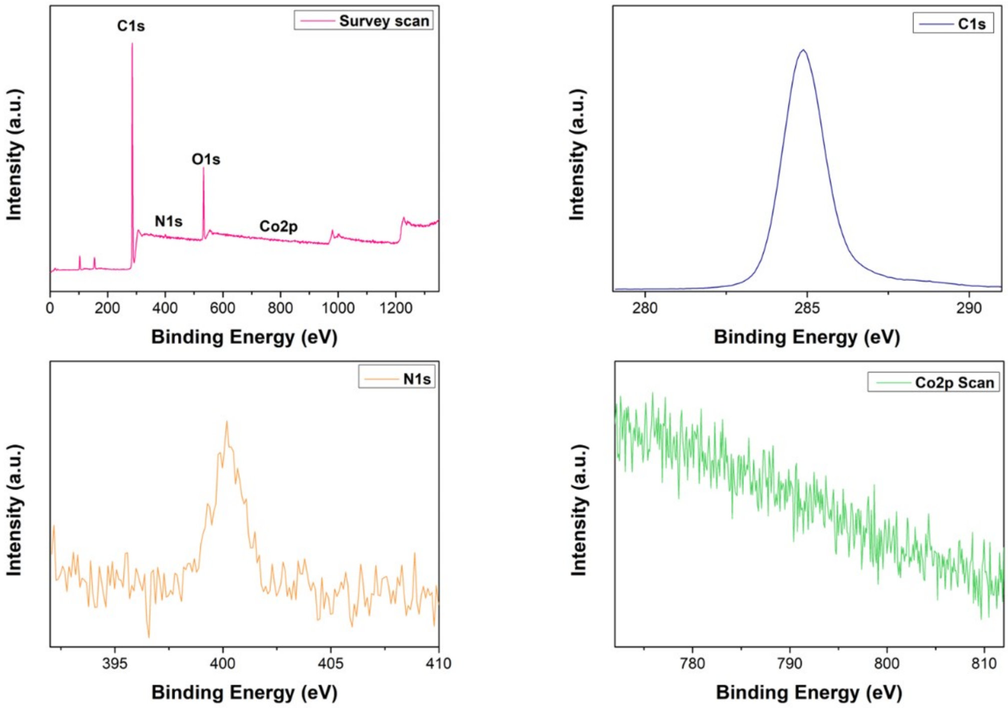

Figure S12. XPS spectra of **CoPc-cov**

9. Comparison of the amount of total and electrochemically active cobalt atoms in CoPc-cov and CoPc-noncov

Table S2. Comparison of the total and electrochemically active Co atoms concentrations on the CFP surface for **CoPc-cov** and **CoPc-noncov**.

#	Catalyst	Total conc., $*10^{-9}$ mol/cm^2	Active conc. (CV), $*10^{-9}$ mol/cm^2	Active conc. (CV)/ Total conc., %	Active conc. (SWV), $*10^{-9}$ mol/cm^2	Active conc. (SWV)/ Total conc. %
1	**CoPc-cov**	1.51*	0.52	34.4	1.10	72.8
2	**CoPc-noncov**	4.00**	0.40	10.0	0.82	20.5

*Identified using ICP. **Identified using the concentration of the deposition solution.

ICP-MS analysis of CoPc content for CoPc-cov

Inductively coupled plasma mass spectrometry (ICP-MS) analysis of **CoPc-cov** was conducted using the following procedure. The **CoPc-cov** electrode was burnt in crucibles by heating it to 850 °C for 2 h. After cooling, the ashes were mixed with 5 mL of 0.25 M HNO_3, and the resulting mixture was filtered through a microporous syringe filter. The Co content of the clear solution was analyzed using Agilent 7500. The measurement of pristine CFP Co content was used as a zero point. Standard solutions for calibration (4, 16, 24, 32, and 40 μg/L) were prepared by diluting certain volumes of the Co^{2+} stock solution (1000±2 mg/L, Sigma Aldrich) in 0.25 M HNO_3. The deionized water and nitric acid were distilled before use.

10. VF-SWV map of CFP

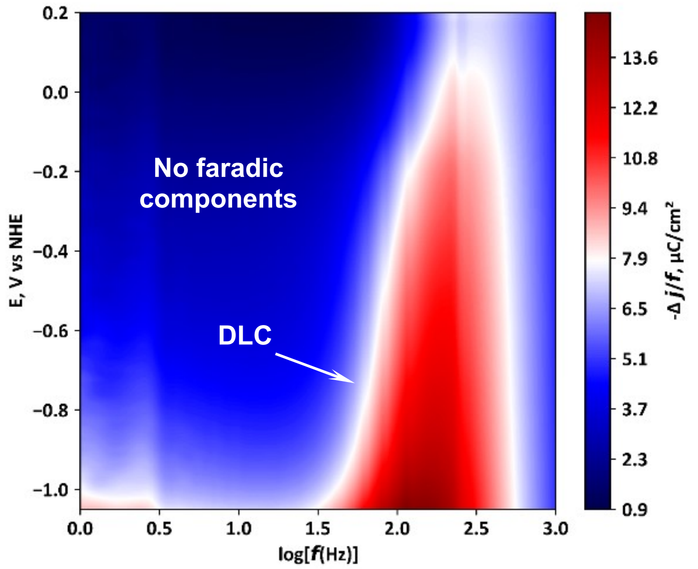

Figure S13. VF-SWV map of the bare CFP. The response of the non-faradic current is the only feature.

11. Simulated VF-SWV maps of CoPc-cov and CoPc-noncov

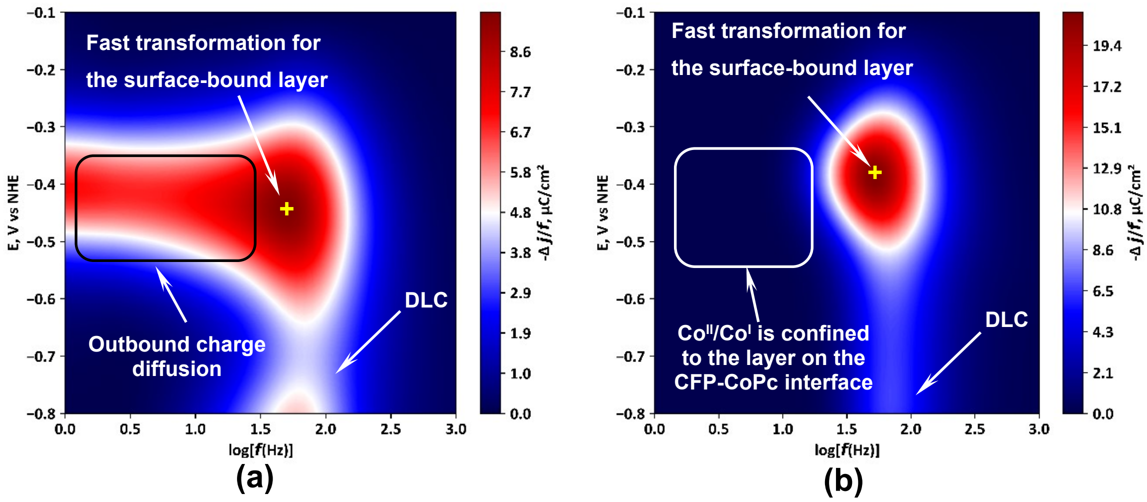

Figure S14. VF-SWV colormaps computed for (**a**) **CoPc-cov** and (**b**) **CoPc-noncov** using the kinetic distributions.

12. Energy of CoPc-CoPc system depending on the multiplicity

Table S3. The energy of two CoPc molecules connected via C-C bond depending on the multiplicity.

Multiplicity	System Energy, (eV)
Singlet	-839.61
Doublet	-839.78
Triplet	-839.83
Quartet	-839.21

To demonstrate that the electron transfer between two CoPc molecules connected via C-C bond is possible, the highest occupied molecular orbital (HOMO) charge densities of the $[CoPc\text{-}CoPc]^{-1}$ system were calculated. From Figure S15 it is obvious that the negative charge of the HOMO(-1e) is distributed between two molecules with a large portion of it residing on Co atoms.

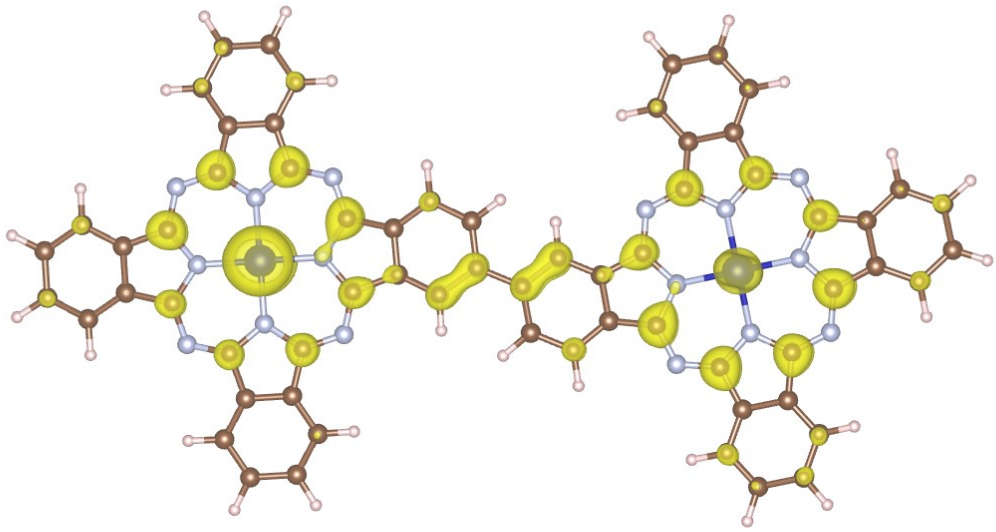

Figure S15. HOMO state for the bonded CoPc-CoPc complex at the most suitable angle for electron transfer (0° dihedral angle) with the net charge of -1e. Calculations for these systems are spin polarised so the charge densities shown are the spin up + spin down charge densities. Yellow regions are areas of charge accumulation.

13. Variation of CoPc-noncov surface loading

The relationship between the CoPc loading and the activity of **CoPc-noncov** in CO_2ERR was assessed (Figure S16). The CoPc was deposited via drop casting of predetermined volumes of $5 \cdot 10^{-5}$ M CoPc solution in the mixture of pyridine (Py) and DMF (10% v/v). The experiment demonstrates that the loading of $4 \cdot 10^{-9}$ mol/cm^2 is optimal for **CoPc-noncov**.

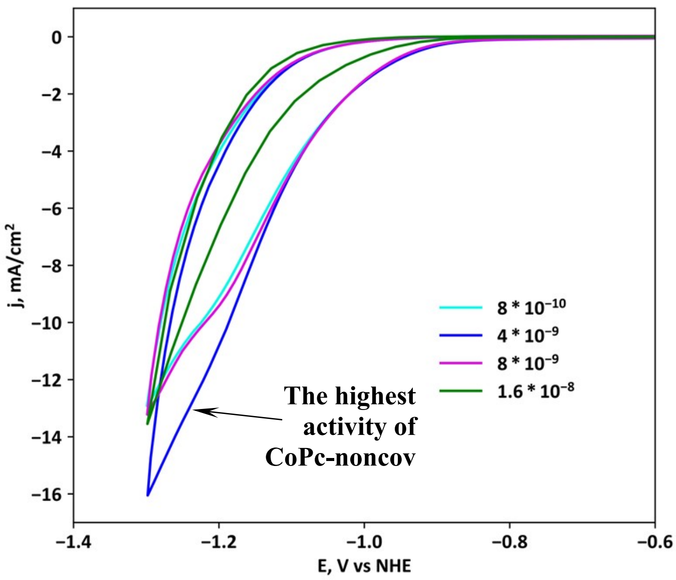

Figure S16. CVs of **CoPc-noncov** with 0.8 (cyan line), 4 (blue line), 8 (violet line), and 16 (green line) nmol/cm^2 of CoPc loaded on the surface of CFP. Electrolyte: CO_2-saturated 0.5 M $KHCO_3$.

14. Comparison of Co-based catalysts

Table S4. Comparison of heterogeneous Pc-based complexes operating in the aqueous medium.

	Catalyst	V vs NHE	Electrolyte	Time, h	*j*, mA/cm^2	FE(CO), %	TOF, s^{-1}	Ref
1	**CoPc-cov**	-1.05	0.5 M $KHCO_3$	24	1.1	82	**9.0**	This work
2	**CoPc-noncov**	-1.05	0.5 M $KHCO_3$	24	0.5	61	3.3	This work
3	CoPc	-1.22	0.5 M $NaHCO_3$	2	2.8	45	N/A	[8]
4	CoPc	-0.69	Nafion 117 membrane	0.5	~60.0	70	0.3	[9]
5	$CoPcF_{16}$	-0.92	0.5 M $NaHCO_3$	2	~1.0	80	0.1	[8]
6	CoPc-CN/CNT	-1.03	0.1 M $KHCO_3$	1	~15.0	98	4.1	[10]
7	CoPc-CN/CNT	-0.89	0.5 M $KHCO_3$	1	~5.6	88	1.4	[10]
8	poly-CoPc/CNT	-0.98	0.5 M $NaHCO_3$	24	12.0	80-90	0.9	[11]
9	CoPc-P4VP	-1.00	0.1 M NaH_2PO_4	2	2.9	92	**6.3**	[12]
10	CoTAPc-ZIF-90-4	-1.42	0.5 M $NaHCO_3$	48	13.0	90	2.8	[13]
11	CoPc-py-CNT[a]	-1.04	0.2 M $NaHCO_3$	12	5.5	98	4.9	[14]
12	CoPc-py-CNT[b]	-1.04	0.2 M $NaHCO_3$	12	0.4	90	**30.7**	[14]
13	CoTMAPC@CNT	-1.05	0.5 M $KHCO_3$	12	11.9	98	**102.9**	[15]
14	Ni-CNT-CC	-1.08	0.5 M $KHCO_3$	100	17.5	99	**27.8**	[16]
15	CoPc/OxC[d]	-1.13	0.1 M $NaHCO_3$	1	0.3	80	**113.0**	[17]
16	CoPc@HCS – 6 (0.49 wt%)	-1.26	0.5 M $KHCO_3$	10	20.5	96	**24.2**	[18]
17	COF-367-Co	-1.10	0.5 M $KHCO_3$	4	3.3	91	0.5	[19]
18	COF-367-Co(1%)	-1.10	0.5 M $KHCO_3$	4	0.5	53	2.6	[19]
19	Co - MOF	-1.10	0.1 M $KHCO_3$	7	1.0	76	0.1	[20]
20	Co - SAC	-1.06	0.5 M $KHCO_3$	60	18.1	94	5.1	[21]

[a] CoPc loading is $5\cdot10^{-9}$ mol/cm^2; [b] CoPc loading is $5\cdot10^{-11}$ mol/cm^2. [c] RDE stands for rotating disk electrode.

[d] CoPc loading is $1\cdot10^{-11}$ mol/cm^2

15. Blank experiments

A series of 15 min electrolyses at the potentials ranging from -0.85 V to -1.30 V vs NHE under CO_2 atmosphere were performed for CFP and **Pc-cov** (Fig S15). In both cases, H_2 was the major product of electroreduction, and no CO was detected. Free-base Pc is an active and selective HER catalyst in agreement with the previous report.[22] It produced a higher total amount of H_2 compared to CFP (Fig. S16a). In the meantime, FE(H_2) was comparable for both electrodes at potentials more negative than -1.00 V vs NHE (Fig. S16b).

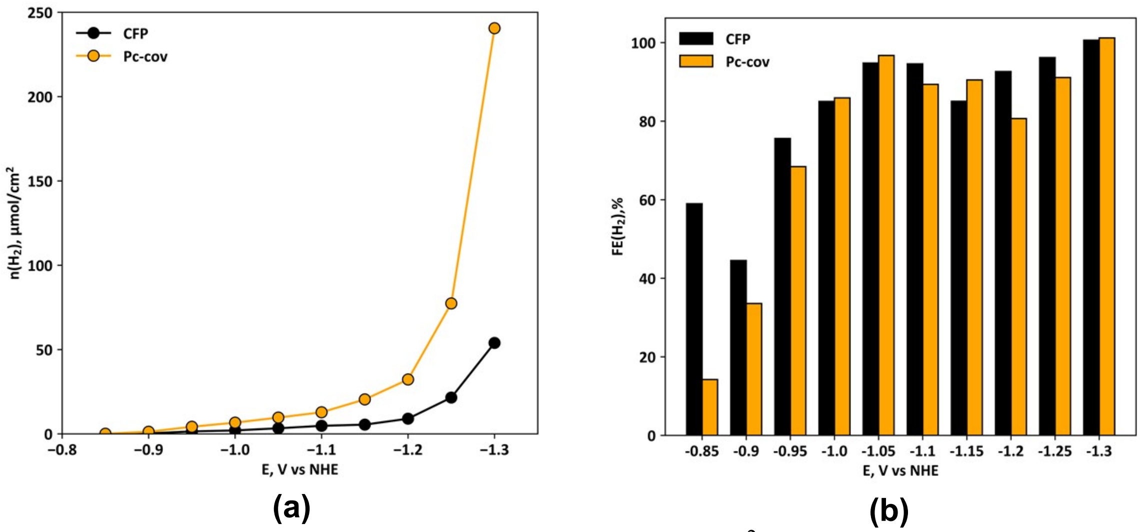

Figure S17. (**a**) The total amount of H_2 produced (µmol/cm^2) and (**b**) FE(H_2) (%) of the bare CFP (black) and CFP modified with **Pc-cov** (orange).

16. Influence of pyridine on the activity of CoPc-cov

The influence of pyridine (Py) was assessed by treating the **CoPc-cov** with DMF:Py (9:1 v/v) for 3 days and comparing its CO_2ERR activity with that of the pristine **CoPc-cov**. Clearly, the overall activity and selectivity of the resulting electrodes are independent of the Py treatment (Figure S18a-b). The reaction mechanisms are also unaffected as the Tafel plots derived both for CO_2ERR and HER are nearly identical (Figure S18c-d).

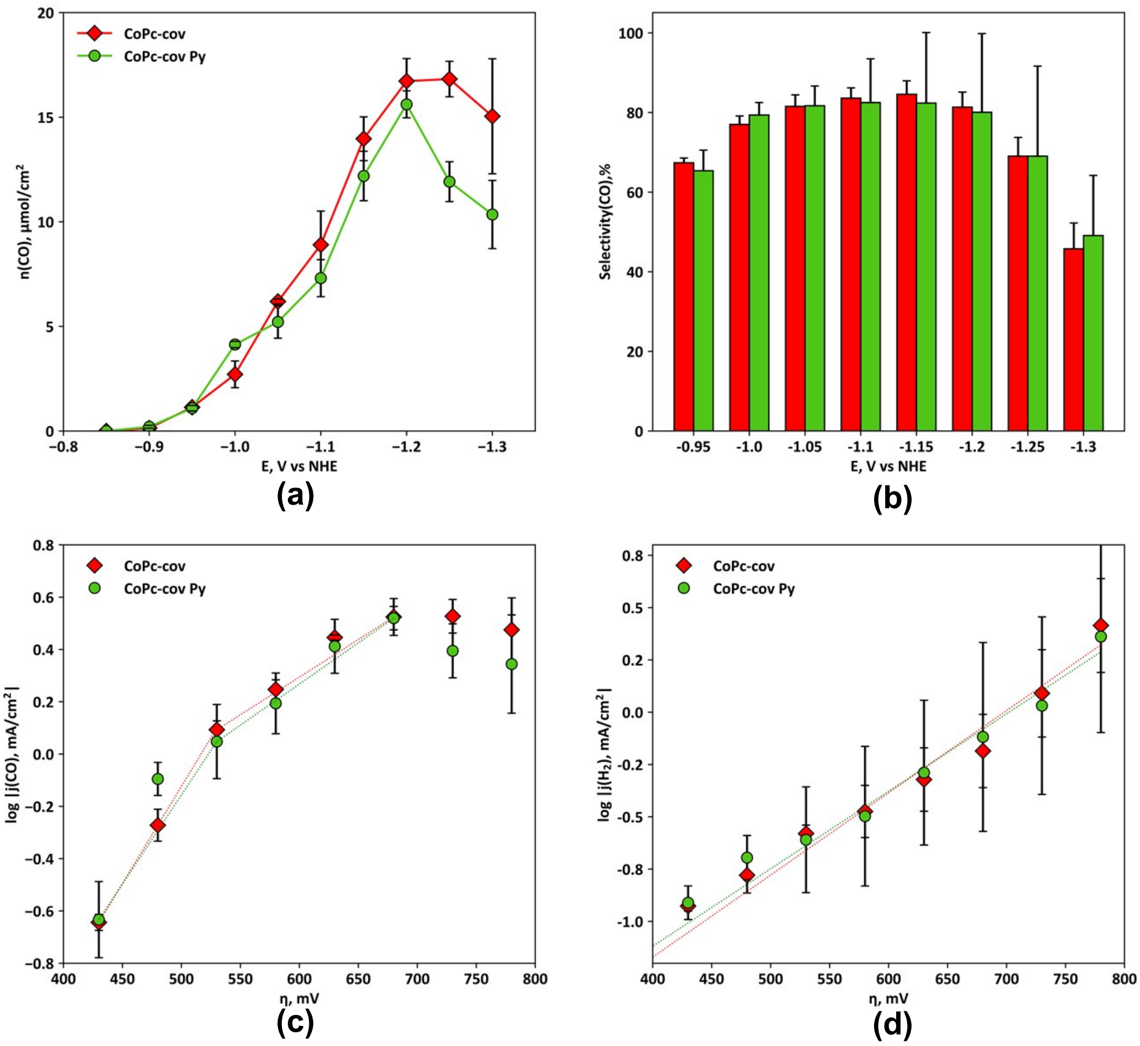

Figure S18. (**a**) Activity, (**b**) CO selectivity, (**c**) Tafel plot of CO_2ERR, and (**d**) Tafel plot of HER recorded for **CoPc-cov** before (red lines and bars) and after (green lines and bars) treatment with DMF:Py (9:1 v/v) mixture. H_2 is the only other product of electrolysis detected and adds up to 100% of selectivity. All electrolyses were performed in 0.5 M $KHCO_3$ under a CO_2 flow of 5 mL/min over 15 min.

17. Assessment of the electrodes after 24 h long CO_2ERR experiments

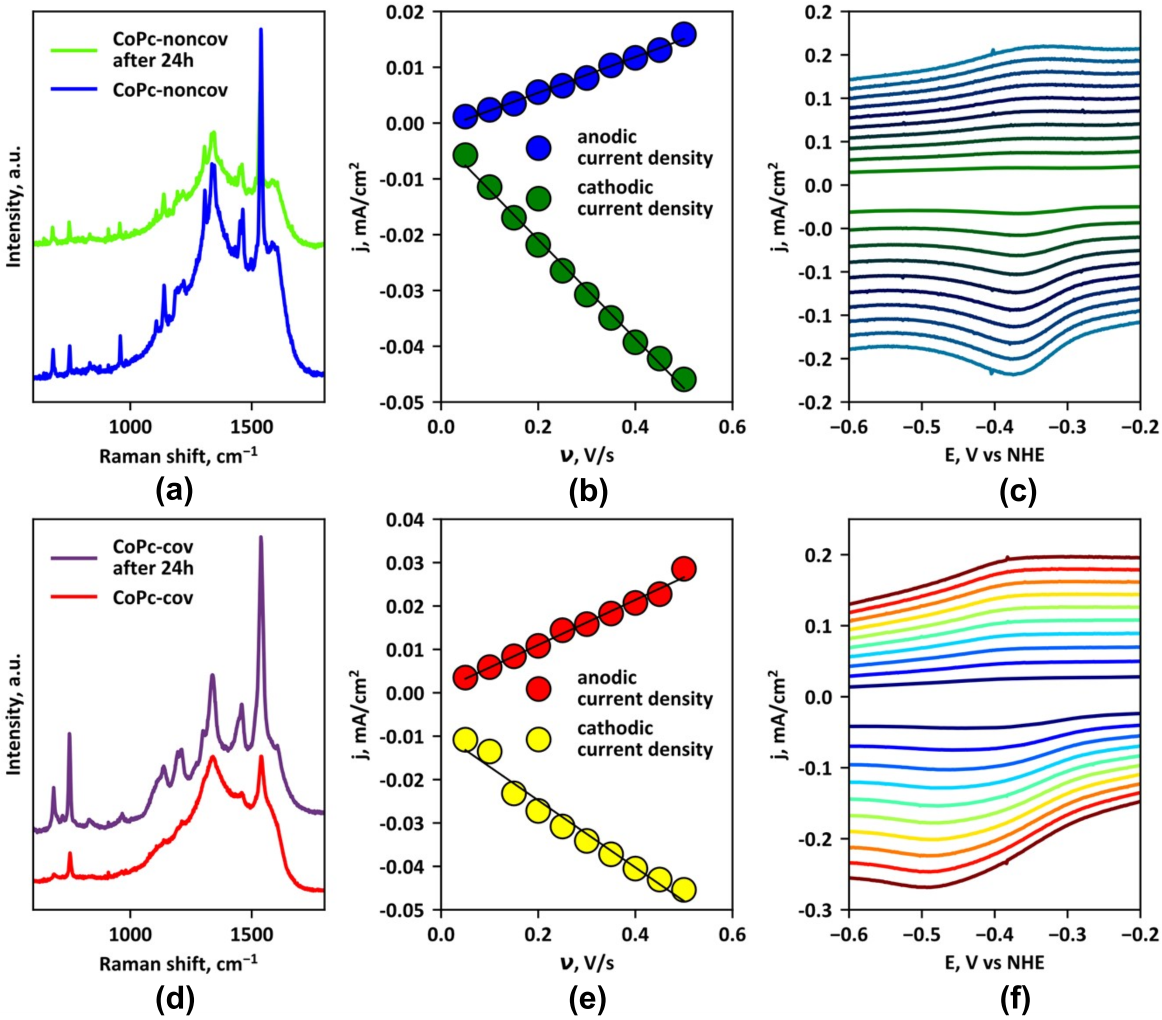

Figure S19. (**a**) Raman spectra of **CoPc-noncov** before and after 24 h electrolysis. (**b**) Dependence of peak current density (**c**) and CV shape on the potential scan rate for **CoPc-noncov** after 24 h experiment. (**d**) Raman spectra for **CoPc-cov** before and after 24 h electrolysis. (**e**) Dependence of peak current density (**f**) and CV shape on the potential scan rate for **CoPc-noncov** after 24 h experiment. CV_S were performed in the degassed 0.1 M KOH.

18. Blank experiment for CoPc-cov and CoPc-noncov

A series of 15-min electrolyses at the potentials ranging from -0.85 V to -1.30 V vs NHE under Ar atmosphere in 0.5 M $KHCO_3$ were performed for **CoPc-noncov** and **CoPc-cov** (Fig S20). In both cases, H_2 was the only product of electroreduction, and no CO was detected. It indicates that no CO was produced as the result of catalyst degradation or reduction of $KHCO_3$.

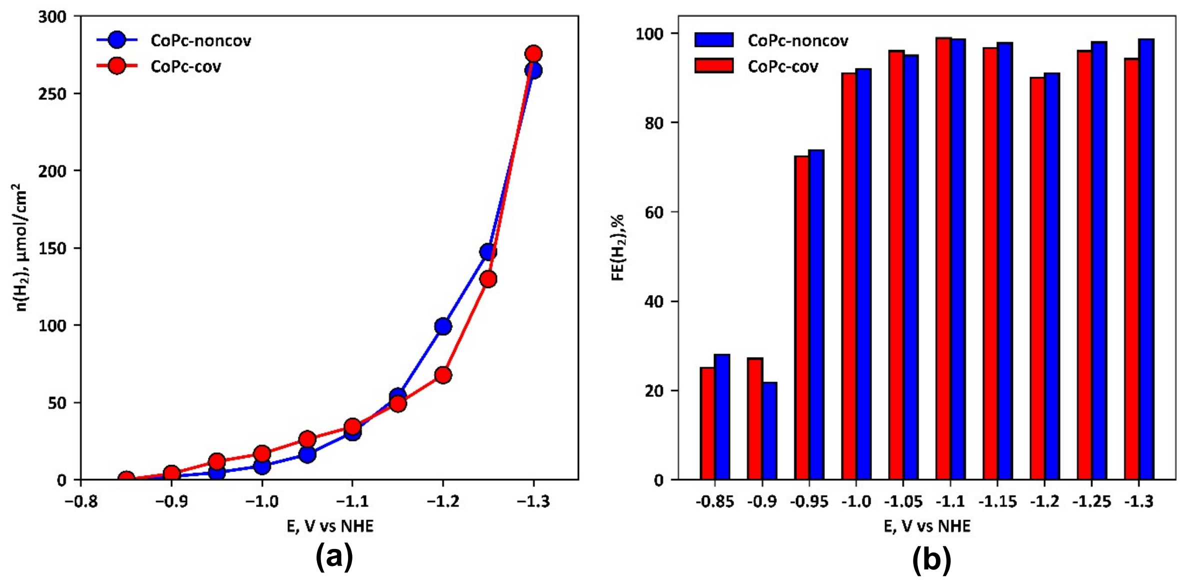

Figure S20. (**a**) The total amount of H_2 produced (µmol/cm^2) and (**b**) FE(H_2) (%) of the CoPc-noncov (blue) and CoPc-cov (red).

19. Results of DFT calculations

Table S5. Comparison of implicit water adsorption energies (eV) of COxx on CoPc.

Catalyst oxidation state	Adsorption Energy (kJ/mol)		
	CO_2	*CO	*COOH
$[Co^{II}(Pc)]$	-16.4	-81.0	-207.4
$[Co^{I}(Pc)]^{-}$	-12.5	-28.9	-120.6
$[Co^{I}(Pc^{\bullet-})]^{2-}$	-33.8	-39.6	-131.2

Table S6. Comparison of bond Length/separation (Å) between COxx and CoPc (implicit water).

Catalyst oxidation state	Bond length/Separation (Å)		
	CO_2	*CO	*COOH
$[Co^{II}(Pc)]$	2.624	2.085	1.884
$[Co^{I}(Pc)]^{-}$	2.110	2.188	1.867
$[Co^{I}(Pc^{\bullet-})]^{2-}$	2.085	1.846	1.853

References

[1] J.-M. Savéant, Elements of Molecular and Biomolecular Electrochemistry, John Wiley & Sons, Inc, (2006) 1-77.
[2] M.M.M. Pelisson, A.D.P. Delega, M. Beltrame, A.R. Simioni, A.C. Tedesco, Synthesis and Photochemical Properties of a bis(n-Hexanoyl)silicon Tribenzonaphthoporphyrazate, Photomedicine and Laser Surgery, 24 (2006) 581-587.
[3] P.J.B. Lester Weinberger, Steven J. Grammatica, Process of preparing phthalocyanine and heterogeneous analogues, Unated States Patent Office 3509146, (1970).
[4] J. Alzeer, P.J.C. Roth, N.W. Luedtke, An efficient two-step synthesis of metal-free phthalocyanines using a Zn(II) template, Chemical Communications, (2009) 1970-1971.
[5] A.N. Marianov, Y. Jiang, Covalent ligation of Co molecular catalyst to carbon cloth for efficient electroreduction of CO_2 in water, Applied Catalysis B: Environmental, 244 (2019) 881-888.
[6] M. Picot, I. Nicolas, C. Poriel, J. Rault-Berthelot, F. Barrière, On the nature of the electrode surface modification by cathodic reduction of tetraarylporphyrin diazonium salts in aqueous media, Electrochem. Comm., 20 (2012) 167-170.
[7] P. Kaur, S.D. Dogra, R. Sachdeva, R. Singh, S. Singh, S.K. Tripathi, G.S.S. Saini, Effect of Pyridine on the Structure and Vibrations of Cobalt Phthalocyanine, Materials Today: Proceedings, 21 (2020) 1809-1817.
[8] N. Morlanés, K. Takanabe, V. Rodionov, Simultaneous Reduction of CO_2 and Splitting of H_2O by a Single Immobilized Cobalt Phthalocyanine Electrocatalyst, ACS Catalysis, 6 (2016) 3092-3095.
[9] I. Yamanaka, K. Tabata, W. Mino, T. Furusawa, Electroreduction of Carbon Dioxide to Carbon Monoxide by Co-pthalocyanine Electrocatalyst under Ambient Conditions, ISIJ International, 55 (2015) 399-403.
[10] X. Zhang, Z. Wu, X. Zhang, L. Li, Y. Li, H. Xu, X. Li, X. Yu, Z. Zhang, Y. Liang, H. Wang, Highly selective and active CO_2 reduction electrocatalysts based on cobalt phthalocyanine/carbon nanotube hybrid structures, Nature Communications, 8 (2017) 14675.
[11] N. Han, Y. Wang, L. Ma, J. Wen, J. Li, H. Zheng, K. Nie, X. Wang, F. Zhao, Y. Li, J. Fan, J. Zhong, T. Wu, D.J. Miller, J. Lu, S.-T. Lee, Y. Li, Supported Cobalt Polyphthalocyanine for High-Performance Electrocatalytic CO_2 Reduction, Chem, 3 (2017) 652-664.
[12] Y. Liu, C.C.L. McCrory, Modulating the mechanism of electrocatalytic CO_2 reduction by cobalt phthalocyanine through polymer coordination and encapsulation, Nature Communications, 10 (2019) 1683.
[13] Z. Yang, X. Zhang, C. Long, S. Yan, Y. Shi, J. Han, J. Zhang, P. An, L. Chang, Z. Tang, Covalently anchoring cobalt phthalocyanine on zeolitic imidazolate frameworks for efficient carbon dioxide electroreduction, CrystEngComm, 22 (2020) 1619-1624.
[14] M. Zhu, J. Chen, R. Guo, J. Xu, X. Fang, Y.-F. Han, Cobalt phthalocyanine coordinated to pyridine-functionalized carbon nanotubes with enhanced CO_2 electroreduction, Applied Catalysis B: Environmental, 251 (2019) 112-118.
[15] J. Su, J.-J. Zhang, J. Chen, Y. Song, L. Huang, M. Zhu, B.I. Yakobson, B.Z. Tang, R. Ye, Building a stable cationic molecule/electrode interface for highly efficient and durable CO2 reduction at an industrially relevant current, Energy & Environmental Science, 14 (2021) 483-492.
[16] S. Liu, H.B. Yang, S.-F. Hung, J. Ding, W. Cai, L. Liu, J. Gao, X. Li, X. Ren, Z. Kuang, Y. Huang, T. Zhang, B. Liu, Elucidating the Electrocatalytic CO_2 Reduction Reaction over a Model Single-Atom Nickel Catalyst, Angewandte Chemie International Edition, 59 (2020) 798-803.

[17] M. Zhu, R. Ye, K. Jin, N. Lazouski, K. Manthiram, Elucidating the Reactivity and Mechanism of CO_2 Electroreduction at Highly Dispersed Cobalt Phthalocyanine, ACS Energy Letters, 3 (2018) 1381-1386.
[18] S. Gong, W. Wang, X. Xiao, J. Liu, C. Wu, X. Lv, Elucidating influence of the existence formation of anchored cobalt phthalocyanine on electrocatalytic CO2-to-CO conversion, Nano Energy, 84 (2021).
[19] S. Lin, C.S. Diercks, Y.-B. Zhang, N. Kornienko, E.M. Nichols, Y. Zhao, A.R. Paris, D. Kim, P. Yang, O.M. Yaghi, C.J. Chang, Covalent organic frameworks comprising cobalt porphyrins for catalytic CO2 reduction in water, Science, 349 (2015) 1208-1213.
[20] N. Kornienko, Y. Zhao, C.S. Kley, C. Zhu, D. Kim, S. Lin, C.J. Chang, O.M. Yaghi, P. Yang, Metal–Organic Frameworks for Electrocatalytic Reduction of Carbon Dioxide, Journal of the American Chemical Society, 137 (2015) 14129-14135.
[21] X. Wang, Z. Chen, X. Zhao, T. Yao, W. Chen, R. You, C. Zhao, G. Wu, J. Wang, W. Huang, J. Yang, X. Hong, S. Wei, Y. Wu, Y. Li, Regulation of Coordination Number over Single Co Sites: Triggering the Efficient Electroreduction of CO_2, Angewandte Chemie International Edition, 57 (2018) 1944-1948.
[22] N. Furuya, K. Matsui, Electroreduction of carbon dioxide on gas-diffusion electrodes modified by metal phthalocyanines, Journal of Electroanalytical Chemistry and Interfacial Electrochemistry, 271 (1989) 181-191.